

Thermalization of Sputtered Particles as the Source of Diffuse Radiation from High Altitude Meteors

Dejan Vinković

*School of Natural Sciences, Institute for Advanced Study, Einstein Drive,
Princeton, NJ 08540, USA*

Abstract

High altitude meteors become luminous at altitudes above ~ 130 km, where the standard ablation theory of meteor light production is not applicable. The physical mechanism responsible for their glow has not been known. We present a model that explains their existence, morphology and lightcurves. The model is based on particles ejected from the meteoroid surface through the sputtering process. The kinetic energy of such a sputtered particle is typically more than 1,000 times larger than the energy of particles in the surrounding atmosphere. Thus the sputtered particle creates a cascade of collisions in the atmosphere during thermalization. We show analytically that this process is capable of producing enough light for detection. We also explain the observed relationship between the beginning height of high altitude meteors and their maximum brightness. In addition, meteors are modeled with a Monte Carlo code developed specifically for this phenomenon. Theoretical images reproduce the observed shapes and sizes of high altitude meteors. Their exact shape depends on the relative angle between the meteor path and observer's line of sight.

Key words: Meteor; Sputtering; High altitude meteors; Monte Carlo; Imaging;

1 Introduction

A meteor is a luminous phenomenon produced by a meteoroid colliding with the earth's atmosphere. The collision starts with atmospheric particles impinging on the meteoroid's body, by which the surface heats up and sublimates.

Email address: dejan@ias.edu (Dejan Vinković).

The cloud of vapor particles surrounding the meteoroid collides further with the atmosphere and becomes ionized and excited. The meteor light is produced by deexcitations, with metals from the meteoroid dominating the spectrum. When the meteor reaches altitudes where the Knudsen number Kn (ratio between the atmospheric mean free path and the meteoroid size) is less than ~ 100 , vapors completely engulf the body and shield it from direct collisions with the atmosphere. After that the heating and evaporation of the meteoroid is caused by hot vapor and radiation from the shock front. During the whole process the meteoroid body is ablating, that is losing mass either as gas or as fragments. The emission of light exists only as a consequence of the ablation process.

The limiting altitude at which most meteors become luminous is ~ 120 km or less, with very few starting at ~ 130 km (e.g. Betlem et al., 2000; Campbell et al., 2000; Brown et al., 2002). The atmospheric mean free path is on the order of meters at these altitudes, which is enough to induce intense evaporation of volatiles from large (centimeters in size) fast meteoroids. It came as surprise, therefore, when meteors of much higher beginning heights were detected in 1995 and 1996 by Fujiwara et al. (1998) using TV cameras. They reconstructed trajectories of two Leonid fireballs of -4^m and -7^m visual magnitude and found that they started at ~ 160 km altitude. This is about 30 km higher than the highest meteors detected by photographic systems (Betlem et al., 2000). The detection was attributed to the much higher sensitivity of TV cameras, especially the infrared region of 900 nm.

This result was confirmed and extended further in 1998 by Spurný et al. (2000a), using high-sensitivity TV systems with limiting magnitude $+6.5^m$. They detected thirteen Leonid fireballs at altitudes above 130km. Three of them were above 180km, with the highest at 200 km. The atmospheric mean free path is over 200 m at an altitude of 200 km, and more than 50 m at 160 km, while the meteoroid body has a size of no more than tens of centimeters for the brightest detected meteors. It is puzzling how meteors can produce light in such conditions. The meteoroid surface is still too cold for sublimation or evaporation and, thus, these *high altitude* meteors can not be explained by the standard theory of meteor ablation.

Spurný et al. (2000b) described the morphological features of these meteors. Initially they appear as a several kilometers big diffuse spot that rapidly transforms into a diffuse comet-like V-shape structure with a head and tail. Sometimes structures like arcs, jets and streamers are visible in the tail. At altitudes of ~ 130 km the meteor changes its appearance into an ordinary droplet-like head shape with trail. This also marks the moment when the standard ablation theory becomes applicable. High altitude meteors up to 150 km were also detected in other meteor streams: η -Aquadrids, Lyrids, and Perseids (Koten et al., 2001).

The decreasing size of the diffuse structure with altitude suggests that the atmospheric mean free path is important as the light is induced by collisions. Spurný et al. (2000a) noted that the beginning meteor height grows with the peak brightness of meteors. This implies that the number of collisions increases with the meteoroid size. Considering these properties of high altitude meteors, we suggest that they are produced by a cascade of collisions in the atmosphere during thermalization of particles sputtered from the meteoroid surface. Sputtering is a process in which an energetic particle projectile ejects atoms from the surface of a solid material. It has been used in meteor physics only to study heating of the surface or slowing down of micrometeoroids (Opik, 1958; Lebedinets et al., 1973; Bronshten, 1983; Coulson, 2002). The luminosity has been associated exclusively with the phase of intense evaporation¹, during which the number of released atoms is increased dramatically (Bronshten, 1983). Unlike vaporization, sputtering can exist at high altitudes because it does not depend much on the meteoroid surface temperature.

It is the purpose of this work to reproduce basic properties of high altitude meteors. We present our 3D Monte Carlo model that traces multiple particle collisions within the atmosphere and show modeling results in the form of theoretical images from a ground-based CCD detector (TV camera).

2 Sputtering from the meteoroid surface

Meteoroids in meteor showers enter the earth’s atmosphere with geocentric velocity ~ 15 km/s to 71 km/s. From the point of view of the meteoroid surface the atmospheric molecules behave like projectiles with kinetic energies of hundreds of eV. For example, an oxygen molecule at 71 km/s has 840 eV of kinetic energy. Collision with the surface dumps this energy into displacements of atoms in the solid until the projectile stops. If the energy is high enough, some atoms are ejected from the surface, and we call these *sputtered particles*. If the projectile exits the solid then we call it a *scattered particle*.

The *sputtering yield* Y is defined as the number of sputtered particles relative to the number of projectiles. The yield depends on the projectile energy, physical and chemical properties of the solid target, and on the type of the sputtered atom. The experimental data on sputtering at the energies of interest here are scarce, thus we mostly rely on numerical models. Since the high altitude meteors detected so far belong to cometary material, we can assume that they are made of a fragile (low binding energy) amorphous material.

¹ During the preparation of this manuscript, we became aware of a study by Hill, Rogers & Hawkes (accepted for publication in *Earth, Moon, and Planets*) describing sputtering as a possible source of luminosity in high altitude meteors.

Calculations show that sputtering yields on such targets approach $Y=1$ for projectile energies of hundreds of eV and that the sputtered atoms have typically 5-10% of the impact energy (Field et al., 1997). In the case of silicates typically present in interstellar grains, the yield can be one or two orders of magnitude smaller (May et al., 2000). Since in this work we do not investigate details of the meteor spectrum, we do not differentiate between different species of sputtered particles. We focus only on the number of particles originating from the surface, and therefore describe both sputtered and scattered particles with Y .

The velocity of sputtered and scattered particles has one component equal to the meteoroid velocity. An additional (smaller) component is present because a particle picks up some additional energy from the impact. The total velocity is a vector sum of those two components. This makes it about 100 times faster than the average thermal speed in the atmosphere. Such a fast particle will create a cascade of collisions before slowing down to the thermal level. During this process of thermalization, collisions will excite atoms and dissociate molecules, which results in production of light by deexcitations.

We make an estimate of whether this process creates enough light to be detected by the TV cameras used in the observations of high altitude Leonid meteors. During the time exposure Δt of one video frame, a meteor of velocity v_m travels a distance $v_m \Delta t$. The number of collisions with atmospheric particles is then $R_m^2 \pi v_m \Delta t n_{\text{atm}}$, where R_m is the meteoroid radius and n_{atm} is the atmospheric number density. Each particle originating from the meteoroid surface will result in many photons from excited (mostly atmospheric) atoms in the cascade. The total number of emitted photons is

$$N_{\text{photon}}^{\text{tot}} = \gamma Y R_m^2 \pi v_m \Delta t n_{\text{atm}}, \quad (1)$$

where γ is the total number of emitted photons in *one* cascade.

These photons are emitted within the overall volume of $\sim 4\pi(L/2)^3/3$, where high altitude meteors have size, L , of several kilometers. On the other hand, one pixel in the CCD of a TV camera covers only a fraction of the meteor angular size on the sky. Spurný et al. (2000a) used an imaging setup with angular pixel size $\sim 2.5'' \times 2.5''$. This covers an area, A , of $150 \times 150 \text{ m}^2$ at 200 km distance. One pixel collects photons from the volume AL . If photons are emitted uniformly within the volume of the meteor, and assuming a meteor size of $L=10 \text{ km}$, the fraction of photons contributing to the flux measured in one pixel is $\Psi = 24A/4\pi L^2 \sim 0.0004$. However, photons are not emitted uniformly, but with a radial gradient. The central region, which we recognize as the meteor head, can emit ~ 100 times more photons than the average, as we will see in §4 from numerical models. This puts the estimate on Ψ closer to 4%.

If the average photon energy is E_0 then the measured flux in one pixel is

$$F_m = \frac{\Psi E_0 N_{\text{photon}}^{\text{tot}}}{4\pi D^2 \Delta t}, \quad (2)$$

where D is distance to the meteor. To work in units of stellar magnitudes, we compare this flux with the flux of Sirius, F_{Sirius} . Although the exact stellar magnitude depends on the spectral sensitivity of the detector, we assume here a visual magnitude of -1^m for Sirius. The apparent meteor magnitude is then

$$\mathfrak{M} = -1^m - 2.5 \log \left(\frac{\gamma Y R_m^2 v_m n_{\text{atm}} \Psi E_0}{4D^2 F_{\text{Sirius}}} \right). \quad (3)$$

Spurný et al. (2000a) and Fujiwara et al. (1998) argue that the sensitivity of TV cameras to wavelengths of ~ 800 nm is one of the reasons why they can detect high altitude meteors. Photons of that wavelength have $E_0 = 2.5 \times 10^{-19}$ J. One collisional cascade can produce $\gamma \sim 100$ photons (see §4), as a product of excitation by collisions or dissociation of molecules. The highest Leonid detected by Spurný et al. (2000a) had $R_m = 0.07$ m and was first detected at distance $D \sim 200$ km. By using $v_m = 71$ km/s for Leonids, $n_{\text{atm}} \sim 10^{16}$ m $^{-3}$ and $F_{\text{Sirius}} \sim 2 \times 10^{-8}$ W/m 2 (integrated flux within the sensitivity range of the camera), our estimate of the brightness is $\mathfrak{M} \sim 6.5^m$. This is exactly the limiting magnitude of the video system used by Spurný et al. (2000a).

For a given observational setup, the limiting magnitude is, by definition, the same as the meteor brightness at the beginning height, H_{begin} . Equation 3 shows that H_{begin} depends on the meteoroid size. Larger meteoroids reach higher maximum brightness $\mathfrak{M}^{\text{max}}$ during their disintegration below ~ 90 km, thus a correlation between these two parameters is to be expected. Indeed, observations show that H_{begin} is higher for brighter meteors (figure 1). In addition to the meteoroid size R_m and distance to the beginning point D , this dependence comes from variables in equation 3 that differ in two meteors from the same meteor stream. The size of a meteor scales with the atmospheric mean free path l_{atm} , thus $\Psi \propto l_{\text{atm}}^{-2}$. For altitudes between 160 km and 200 km, the atmosphere has $l_{\text{atm}} \propto \exp(H_{\text{begin}}/27.3\text{km})$ and $n_{\text{atm}} \propto \exp(-H_{\text{begin}}/26.8\text{km})$ (the U.S. Standard Atmosphere 1976).

In the single body approximation of ablation, the maximum meteor brightness $\mathfrak{M}^{\text{max}}$ in magnitudes is (see Appendix)

$$\mathfrak{M}^{\text{max}} = -7.5 \log R_m - 2.5 \log(\cos Z) + \text{constant}, \quad (4)$$

where Z is the zenith angle of the meteoroid's trajectory. Combining this with

equation 3 yields the dependence of H_{begin} on \mathfrak{M}^{max} :

$$H_{begin} = -5.55\text{km} [\mathfrak{M}^{max}] + \text{constant}, \quad (5)$$

where $[\mathfrak{M}^{max}]$ is the *reduced maximum brightness*:

$$[\mathfrak{M}^{max}] = \mathfrak{M}^{max} + 7.5 \log\left(\frac{D}{200\text{km}}\right) + 2.5 \log(\cos Z) \quad (6)$$

scaled to the distance of 200 km.

Observed values of H_{begin} as a function of $[\mathfrak{M}^{max}]$ are plotted in figure 2. Linear regression gives a slope of -5.9 ± 0.5 km, which agrees with the theoretical slope in equation 5.

3 Monte Carlo model

Unusual morphology is another characteristic of high altitude meteors. In order to explain changes in their appearance with altitude, we performed Direct Simulation Monte Carlo (DSMC) modeling. The simulation follows a sputtered particle and all high velocity particles produced by collisions during the thermalization process. The three-dimensional distribution of collisions provides information on the spatial distribution of photons produced.

Although DSMC is widely used for modeling interactions between rarefied gases and solids, including reentry of spacecraft (Oran et al., 1998), it has very rarely been used in meteor physics. Boyd (2000) modeled the flow around a 1 cm Leonid meteor at 95 km altitude. The model shows that meteoroid vapors surround the body and interact with the atmosphere on a larger scale than when the vapors are not produced. This confirms theoretical expectations of vapor shielding. Zinn et al. (2004) also performed, but not with Monte Carlo, a numerical study of Leonids at these and lower altitudes with a hydrodynamics code coupled with radiative transfer. They found that the meteoroid vapors are stopped very quickly by the air and moved into the meteor wake, where the vapor-air mixture expands and cools. This stopping process is the dominant source of energy deposition in the atmosphere. These models demonstrate the importance of correct numerical treatment of the vapor cloud.

All these numerical models have been applied to conditions in which $\text{Kn} < 10$, typically for altitudes below ~ 100 km. This is where the intense vaporization and compressed air in front of the meteoroid create conditions appropriate for the approximation of vapor shielding and the continuous flow regime. This choice of flow conditions is also influenced by the numerical codes used in

simulations. They are not designed specifically for meteors and their applicability requires the hydrodynamic fluid regime. In contrast, our DSMC code is written and designed specifically for meteors under the molecular flow regime at higher altitudes.

In this study we focus solely on the sputtering effect at altitudes above ~ 130 km as relevant to high altitude meteors. For simplicity, we do not differentiate between different atomic and molecular species. Other physical processes (like vaporization, ionization, dissociation, excitation, chemistry, etc.) can be added in the future to expand the applicability of the code. The Monte Carlo methodology used in the code is described by Xie and Mumma (1996) for the case of cometary atmospheres. Our modifications are related to the physical conditions in the earth's atmosphere and the sputtering process. Here we describe the basic numerical procedure, while for the detailed description we refer to the original paper.

The numerical simulation follows the flight of a meteoroid through the atmosphere and calculates how many particle collisions with the air happen during one time step δt of calculation. Each modeled particle in DSMC is a statistical representative of a set of particles. For N_{MC} model particles within time step δt at altitude H , the number of real particles in one set is

$$N_{\text{set}}(H) = \frac{R_m^2 \pi v_m n_{\text{atm}}(H) \delta t(H)}{N_{\text{MC}}}. \quad (7)$$

If δt is held constant during the simulation then the distance covered by the meteor during one time step would eventually become much larger than the atmospheric mean free path l_{atm} . In order to avoid this statistical problem, we move the meteoroid one l_{atm} per step, thus $\delta t(H) = l_{\text{atm}}(H)/v_m$. The number of Monte Carlo particles used in our computations is $N_{\text{MC}}=1500$.

A model particle is ejected in a random direction from a random location on the meteoroid surface. We use a spherical meteoroid of $R_m=0.05$ m and isotropic sputtering for simplicity. A more general shape and sputtering angle distribution could be used in the future. We also assume a constant sputtering velocity V_{sp} of 20 km/s relative to the meteoroid. This corresponds to $\sim 10\%$ of the collision energy if the masses of projectiles and sputtered particles are equal. We plan to introduce a more realistic distribution of sputtered velocities, such as a Maxwellian (Coulson, 2002) or Sigmund-Thompson (Thompson, 1968; Sigmund, 1969).

The history of collisions of an ejected particle and all subsequent collisionally produced fast air particles is recursively traced by the code. The basic assumption is that fast particles collide only with the background atmosphere, but never with each other. This is a good approximation as long as the local

number density of ejected particles around the meteoroid is not comparable to the atmospheric density. This condition is satisfied in our case of sputtered particles.

Since all modeled particles are treated as the same species, there is only one collisional cross section σ . We use the Variable Hard Sphere model where the cross section is velocity dependent:

$$\sigma = \sigma_{\text{ref}} \left(\frac{v_{\text{ref}}}{v} \right)^s. \quad (8)$$

We use the reference values typical for air: $s=0.25$, $\sigma_{\text{ref}}=1.26 \times 10^{-19} \text{m}^2$ and $v_{\text{ref}}=(4989/M)^{0.5} \text{m/s}$ (Boyd, 2000), where M is the molar mass (kg/mol) of air at the altitude of collision. The time between collisions for a particle of velocity v is calculated from a random number \mathfrak{R} between zero and one:

$$t_{\text{coll}} = \sum_H \Delta t(H). \quad (9)$$

$$\ln(\mathfrak{R}) = - \sum_H \Delta t(H) \sigma v n_{\text{atm}}(H)$$

This was derived from the assumption that air particles, whose velocities are much smaller than the velocity of modeled particles, follow the Maxwellian distribution. The sum over $n_{\text{atm}}(H)$ is introduced because the atmospheric density is changing with altitude along the particle trajectory. To describe this change we use altitude steps of 1 km. The time that the particle spends crossing an altitude layer is $\Delta t(H)$. Since neither t_{coll} nor H is known in advance, the equation is solved iteratively.

A collision between particles requires random selection of the velocity vector v_t of an air particle in the Maxwellian distribution. We choose cylindrical coordinates $(\varphi_t, v_{\rho t}, v_{z t})$ where

$$\vec{v}_t = v_{\rho t} \cos \varphi_t \hat{i} + v_{\rho t} \sin \varphi_t \hat{j} + v_{z t} \hat{k}. \quad (10)$$

From three random numbers \mathfrak{R}_1 , \mathfrak{R}_2 and \mathfrak{R}_3 , the velocity is given as:

$$\varphi_t = 2\pi \mathfrak{R}_1 \quad (11)$$

$$v_{\rho t} = \bar{v} \sqrt{-\ln \mathfrak{R}_2} \quad (12)$$

$$\text{Erf} \left(\frac{|v_{z t}|}{\bar{v}} \right) = 2|\mathfrak{R}_3 - 0.5| \quad (13)$$

$$\text{sign}(v_{z t}) = \text{sign}(\mathfrak{R}_3 - 0.5),$$

where Erf is the Error integral, $\bar{v}^2=2RT(H)/M(H)$, and $T(H)$ and $M(H)$ are the temperature and molar mass of the air at altitude H . The collisional scattering of two particles is isotropic, with velocity directions chosen randomly in the center-of-mass frame. When the kinetic energy of a particle drops below some pre-defined limit (10 eV in our simulations), its trajectory and collisions are not traced any more. This limit cannot be below the energy of photons that we expect to be produced. Another reason for losing a particle is collision with the meteoroid. We do not consider sputtering from such secondary collisions.

4 Model results

In order to visualize a meteor, we collect the total number of collisions visible from the ground by a TV camera at location \vec{r}_{cam} . The coordinate system is shown in figure 3. The meteor's direction of flight is $\hat{v}_m = -\sin Z \hat{j} - \cos Z \hat{k}$, where Z is the zenith angle (45° in our model). The camera's frames point at subsequent locations along the meteor path in order to track the meteor flight. When a collision happens at \vec{r}_{coll} in space and t_{coll} in time (starting from the first frame), the camera's frame number f_{cam} is calculated (by ignoring decimal places) from

$$f_{\text{cam}} = \frac{t_{\text{coll}} + |\vec{r}_{\text{coll}} - \vec{r}_{\text{cam}}|/c}{\Delta t} \quad (14)$$

where c is the speed of light. The number of collisions in one set N_{set} (equation 7) is added to the image pixel that points at the collision.

The first appearance of the meteor depends on the camera's sensitivity. The pixel values can be transformed into apparent magnitudes if we define the frame in which the meteor first appears. This is the frame showing the meteor at its beginning height H_{begin} . The brightest pixel in that frame is set to be the limiting magnitude $\mathfrak{M}_{\text{limit}}$ and its value, N_{limit} , is used for calculating the apparent magnitude. If the distance of the meteor from the camera in this first frame is D_{limit} then the brightness of a pixel is

$$\mathfrak{M} = \mathfrak{M}_{\text{limit}} - 2.5 \log \left[\left(\frac{D_{\text{limit}}}{D} \right)^2 \frac{N_{\text{collisions}}}{N_{\text{limit}}} \right], \quad (15)$$

where $N_{\text{collisions}}$ is the pixel value and D is the meteor's distance.

Figure 4 shows images of our meteor model from four different camera locations. The basic morphological features described by Spurný et al. (2000b) are

successfully reproduced. The meteor first appears as a diffuse structure that grows in size, but then turns into a comet-like V-shape, followed by a transition into a more compact, elongated structure. The exact shape depends on the relative position between the camera and the meteor path. Since we do not consider photon emission from long-lived atomic states, the feature missing at lower altitudes, below ~ 140 km, is the train that develops behind the meteor. Figure 4 also shows the number of collisions “visible” by each pixel. Collisions are concentrated at the center of the diffuse structure, which demonstrates the plausibility of the value used for Ψ in equation 3.

The efficiency of light production in high altitude meteors (described as γ in equation 3) depends on the number of collisions. Collisional cascades differ in their total number of collisions. This number is mostly between 100 and 200, with ~ 180 collisions being the most frequent (figure 5). The total energy of collision between two particles follows the distribution $dN = Nf(E)dE$ that can be calculated from

$$f(E) = \frac{\Delta N}{\Delta E N}, \quad (16)$$

where ΔN and ΔE are small increments in the number of collisions and collisional energy, and the total number of collisions is N . The distribution obtained is shown in figure 6. For most of its range it has the functional dependence $f(E) \propto E^{-p}$, with $p=0.66$.

From the meteoroid’s point of view, the diffuse coma does not change much with altitude when measured in the units of atmospheric mean free path l_{atm} . Figure 7 shows the meteor viewed by a camera that moves with the meteor. Since collisions between the fast coma particles are not considered, the size of the coma is controlled exclusively by l_{atm} . Decreasing altitude only increases the number of collisions per unit volume. If the assumption of negligible coma-coma interactions holds all the way to the end of the molecular flow regime, then the meteor would shrink to a few meters in size at 120 km altitude, and below one meter at ~ 100 km. The fact that the observed meteor size is larger at these altitudes indicates that the coma eventually becomes dense enough to produce internal collisions. In addition, vaporization starts to produce particles in larger numbers than sputtering, making the coma denser than during sputtering.

Meteor images based on apparent magnitudes (upper rows in figure 4) can be used to calculate the meteor light curve. Total meteor brightness is the sum of all pixels brighter than the limiting magnitude. Hence the absolute meteor

magnitude, defined as the brightness at 100 km distance, is

$$M = \mathfrak{M}_{\text{limit}} - 2.5 \log \left(\frac{D_{\text{limit}}}{100\text{km}} \right)^2 - 2.5 \log \left(\sum_{m_{\text{pix}} < 6.5^m} \frac{N_{\text{collisions}}}{N_{\text{limit}}} \right), \quad (17)$$

where m_{pix} is the pixels' apparent magnitude. Since M is a function of D_{limit} , the light curve depends on the beginning height H_{begin} and on the camera's position. The dependence on H_{begin} is stronger, because N_{limit} is a function of altitude. Notice that according to equation 3, N_{limit} is a constant for a given meteor and detector. By letting N_{limit} vary with altitude, we declare it an unknown that can be determined experimentally from the pixel value of the limiting magnitude in the first meteor frame.

Figure 8 shows the light curves of our meteor model for two beginning heights: 200 km and 171 km. The cameras have different distances to the starting point of the meteor, thus they differ in the absolute magnitude at H_{begin} . In the first few frames, the meteor brightness is slightly erratic as the meteor is a few pixels in size and susceptible to stochastic variations in pixel values. After that the light curve smoothes out, but it is not linear; it shows a change in slope, which is also an observed characteristic of high altitude meteors (Spurný et al., 2000b).

5 Conclusion

We have shown that thermalization of particles sputtered from a meteoroid surface by the impinging atmosphere can explain the phenomenon of high altitude meteors. A sputtered particle has a much larger kinetic energy than the surrounding atmospheric particles. It takes between 100 and 200 collisions between particles in the resulting collisional cascade to redistribute this initial energy down to the thermal level of the atmosphere. The volume filled with collisions surrounding the meteoroid is controlled by the atmospheric mean free path. These collisions are the source of the atomic excitations required for the light production.

We showed that this process can create enough photons to be detected by high-sensitivity TV cameras. The number of sputtered particles, and consequently the number of photons produced, is proportional to the meteoroid size. This explains why the observed beginning height correlates with the maximum meteor brightness. Our analytical description of this correlation agrees with the data. We developed a Monte Carlo code specifically for the problem of high altitude meteors. Simulations successfully reproduced the observed size and morphology of these meteors. We found that their shape also depends on

the relative angle between the meteor path and the camera’s line of sight.

This model provides the grounds for further study of meteoroid properties and meteor microphysics. Features like streams and jets observed in high altitude meteors are probably created by nonuniform sputtering and meteoroid rotation. This will be addressed in the future by Monte Carlo modeling. It is also possible to trace different atomic species during thermalization, which is a highly nonequilibrium process, and to calculate their spectral lines. Such numerical simulations will remove the need for “fudge” factors typically used to hide underlying microphysics in meteor equations.

Acknowledgment

This work was supported by NSF grant PHY-0070928. The author would like to thank Peter Jenniskens, SETI Institute, and Bruce Draine, Princeton University, for valuable discussions.

APPENDIX: Maximum brightness from the single body ablation theory

Meteor altitude H is described by the equation of motion:

$$\frac{dH}{dt} = -v_m \cos Z. \tag{18}$$

Ablation is changing the meteoroid mass as:

$$\frac{dm}{dt} \propto n_{\text{atm}}(H)m^{2/3}v_m^3. \tag{19}$$

Combining and integrating these two equations, while keeping the meteor velocity constant (a good approximation for fast meteors like Leonids) and assuming an exponential atmosphere, we get the solution:

$$m^{1/3}(H) = m_m^{1/3} - \text{constant} \times \frac{n_{\text{atm}}(H)}{\cos Z}, \tag{20}$$

where m_m is the initial meteoroid mass. At the end point of the trajectory H_{end} , the meteor mass becomes zero, thus

$$n_{\text{atm}}(H_{\text{end}}) \propto m_m^{1/3} \cos Z. \tag{21}$$

The maximum meteor light intensity is (e.g. Bronshten, 1983; Opik, 1958)

$$I_{\max} \propto m_m^{2/3} n_{\text{atm}}(H_{\text{end}}). \quad (22)$$

Since $m_m^{1/3} \propto R_m$, from equation 22 and 21 it follows that the maximum brightness in magnitudes is

$$\mathfrak{M}^{\max} = -7.5 \log R_m - 2.5 \log(\cos Z) + \text{constant}. \quad (23)$$

References

- Betlem, H., Jenniskens, P., Spurný, P., Van Leeuwen, G. D., Miskotte, K., Ter Kuile, C. R., Zarubin, P., Angelos, C. Precise Trajectories and Orbits of Meteoroids from the 1999 Leonid Meteor Storm. *Earth Moon and Planets* 82, 277-284. 2000.
- Boyd, I. D. Computation of Atmospheric Entry Flow about a Leonid Meteoroid. *Earth Moon and Planets* 82, 93-108. 2000.
- Bronshten, V. A. *Physics of meteoric phenomena*, Dordrecht, D. Reidel Publishing Co., 1983.
- Brown, P., Campbell, M. D., Hawkes, R. L., Theijsmeijer, C., Jones, J. Multi-station electro-optical observations of the 1999 Leonid meteor storm. *Planetary and Space Science* 50, 45-55. 2002.
- Campbell, M. D., Brown, P. G., Leblanc, A. G., Hawkes, R. L., Jones, J., Worden, S. P., Correll, R. R. Image-intensified video results from the 1998 Leonid shower: I. Atmospheric trajectories and physical structure. *Meteoritics and Planetary Science* 35, 1259-1267. 2000.
- Coulson, S. G. Resistance of motion to a small, hypervelocity sphere, sputtering through a gas. *Monthly Notices of the Royal Astronomical Society* 332, 741-744. 2002.
- Field, D., May, P. W., Pineau des Forets, G., Flower, D. R. Sputtering of the refractory cores of interstellar grains. *Monthly Notices of the Royal Astronomical Society* 285, 839-846. 1997.
- Fujiwara, Y., Ueda, M., Shiba, Y., Sugimoto, M., Kinoshita, M., Shimoda, C., Nakamura, T. 1998. Meteor luminosity at 160 km altitude from TV observations for bright Leonid meteors. *Geophysical Research Letters* 25, 285-288. 1998.
- Koten, P., Spurný, P., Borovička, J., Štokr, R. Extreme beginning heights for non-Leonid meteors. *ESA SP-495: Meteoroids 2001 Conference* 119. 2001.
- Lebedinets, V. N., Manochina, A. V., Shushkova, V. B. Interaction of the lower thermosphere with the solid component of the interplanetary medium. *Planetary and Space Science* 21, 1317-1332. 1973.
- May, P. W., Pineau des Forêts, G., Flower, D. R., Field, D., Allan, N. L.,

- Purton, J. A. Sputtering of grains in C-type shocks. *Monthly Notices of the Royal Astronomical Society* 318, 809-816. 2000.
- Opik, E. J. *Physics of meteor flight in the atmosphere.*. New York, Interscience Publishers, 1958.
- Oran, E. S., Oh, C. K., Cybyk, B. Z. Direct Simulation Monte Carlo: Recent Advances and Applications. *Annual Review of Fluid Mechanics* 30, 403-441. 1998.
- Sigmund, P. Theory of Sputtering. I. Sputtering Yield of Amorphous and Polycrystalline Targets. *Physical Review* 184, 383-416. 1969.
- Spurný, P., Betlem, H., van't Leven, J., Jenniskens, P. Atmospheric behavior and extreme beginning heights of the 13 brightest photographic Leonids from the ground-based expedition to China. *Meteoritics and Planetary Science* 35, 243-249. 2000a.
- Spurný, P., Betlem, H., Jobse, K., Koten, P., van't Leven, J. New type of radiation of bright Leonid meteors above 130 km. *Meteoritics and Planetary Science* 35, 1109-1115. 2000b.
- Thompson, M. W., The energy spectrum of ejected atoms during the high energy sputtering of gold. *Philosophical Magazine* 18, 377-414. 1968.
- Xie, X., Mumma, M. J. Monte Carlo Simulation of Cometary Atmospheres: Application to Comet P/Halley at the Time of the Giotto Spacecraft Encounter. I. Isotropic Model. *Astrophysical Journal* 464, 442. 1996.
- Zinn, J., Judd, O. P., Revelle, D. O. Leonid meteor ablation, energy exchange, and trail morphology. *Advances in Space Research* 33, 1466-1474. 2004.

Fig. 1. Beginning heights as a function of the maximum brightness for Leonid meteors. *Diamonds* are observations from Spurný et al. (2000a) and *circles* are from Campbell et al. (2000). Even though these two data sets are from different observational setups, they follow a similar functional dependence indicated by the *solid line*. Two Leonids observed by Fujiwara et al. (1998) are shown as *squares*.

Fig. 2. Beginning heights as a function of the reduced maximum brightness (see equation 6). Only observations from Spurný et al. (2000a), marked as *diamonds*, are used, in order to have the same limiting magnitude for all data. The *solid line* is the linear regression, with the 95% confidence interval shown as *dashed lines*. For comparison, two Leonids observed by Fujiwara et al. (1998) are shown as *squares*.

Fig. 3. Geometry of the modeled meteor and camera positions. The meteor's entry (zenith) angle is 45° in the Y-Z plane and its trajectory points toward the origin of the coordinate system. The cameras' coordinates are: (0,150km,0) for Camera 1, (50km,100km,0) for Camera 2, (100km,50km,0) for Camera 3 and (0,-100km,0) for Camera 4.

Fig. 4. Modeled meteor observed by Cameras 1-4 (see figure 3), respectively, from top to bottom. The *upper* row in each panel shows the meteor brightness in apparent magnitudes (see equation 15) based on the beginning height of 200 km and the limiting magnitude of 6.5^m . The meteor's height and distance from the camera are indicated in each frame, together with the pixel size. The angular size of pixels is $3.75'' \times 3.75''$. The *lower* row in each panel shows the number of particle collisions visible at each pixel in these same camera frames. The meteoroid radius is $0.05 m$.

Fig. 5. Rate of occurrence of the total number of collisions within one collisional cascade, calculated from 100,000 cascades.

Fig. 6. Distribution of collisional energies (see equation 16) during thermalization, calculated from 1.6×10^7 collisions.

Fig. 7. Modeled meteor observed by a camera that follows the meteor. The pixel size, indicated in each frame, is equal to the atmospheric mean free path at the meteoroid altitude. The asymmetry at larger altitudes comes from the variation of the mean free path in the coma.

Fig. 8. Theoretical light curves of the high altitude meteor model for the beginning heights of 200 km and 171 km, observed from four different locations on the ground (figure 3).

Fig.1:

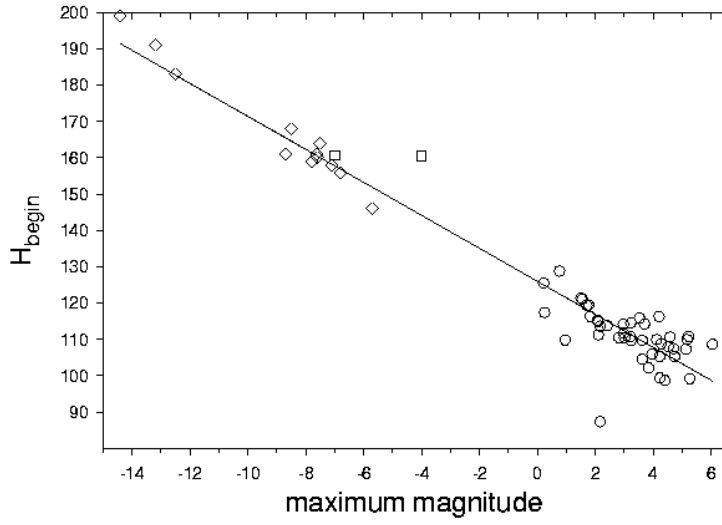


Fig.2:

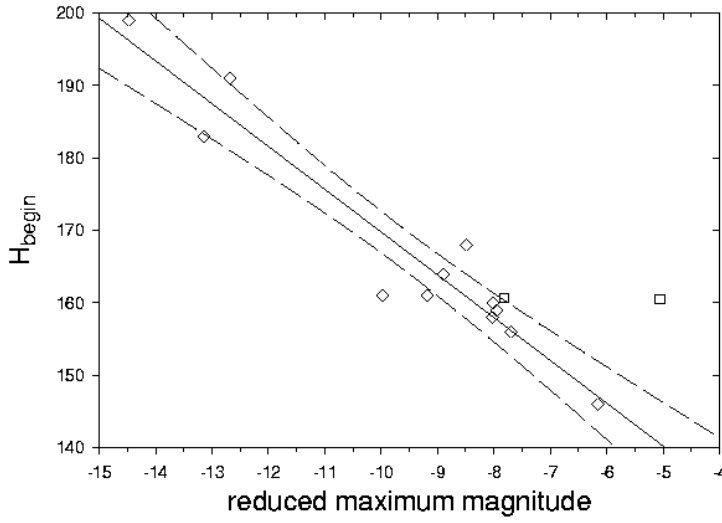


Fig.3:

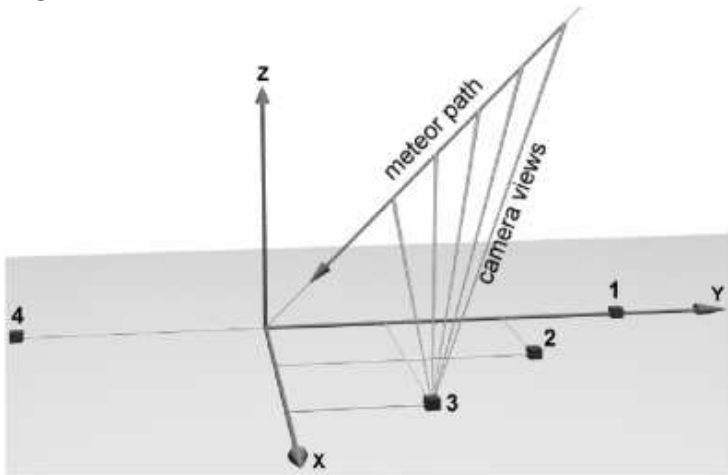


Fig.4:

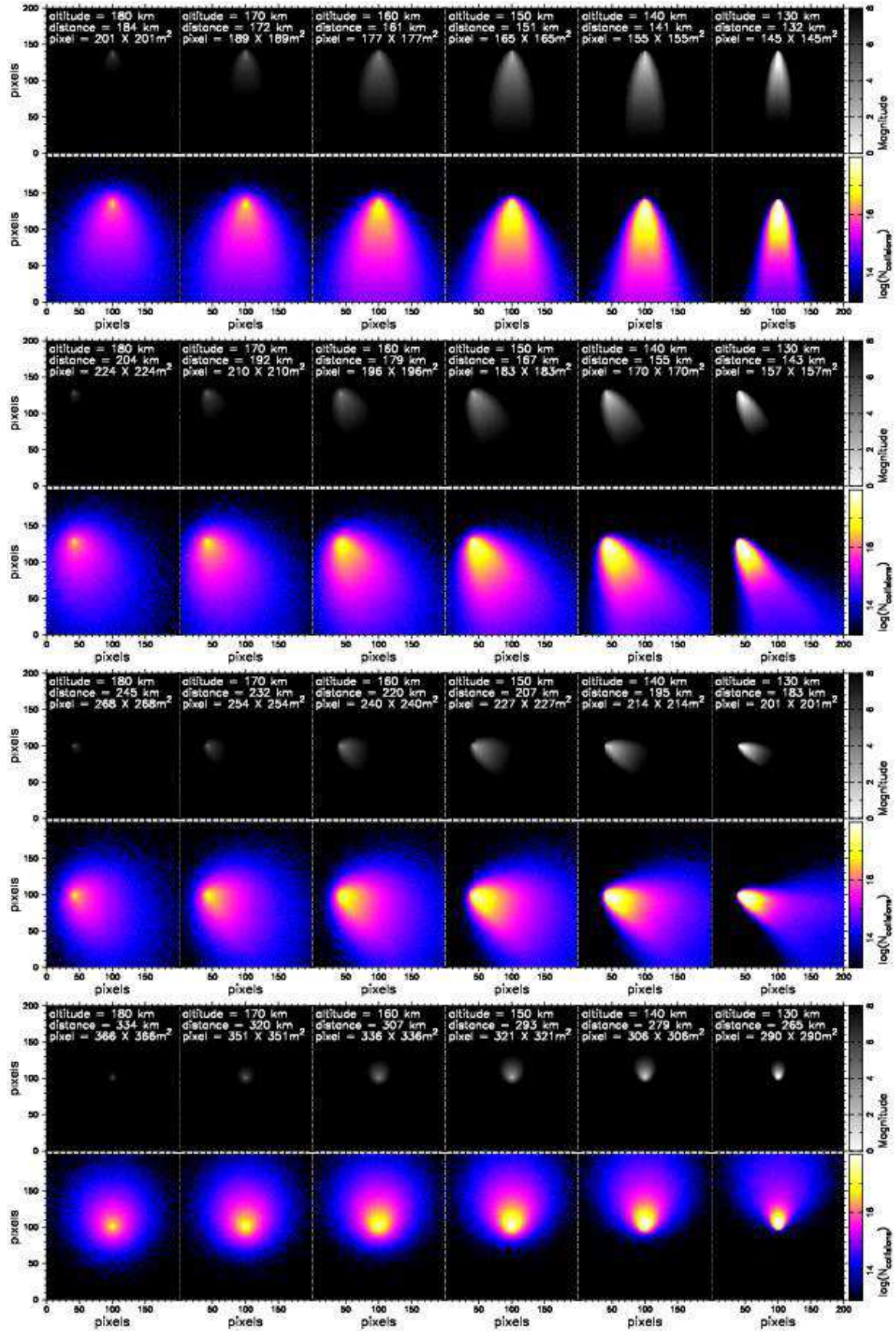


Fig.5:

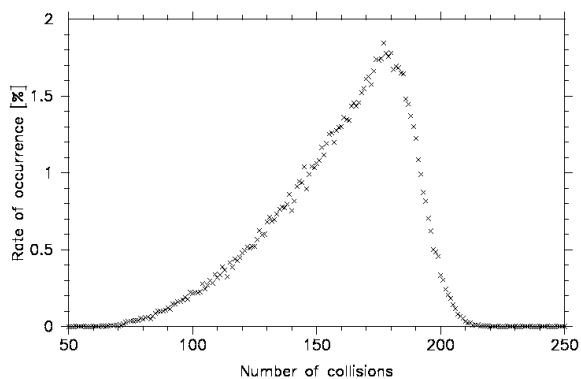


Fig.6:

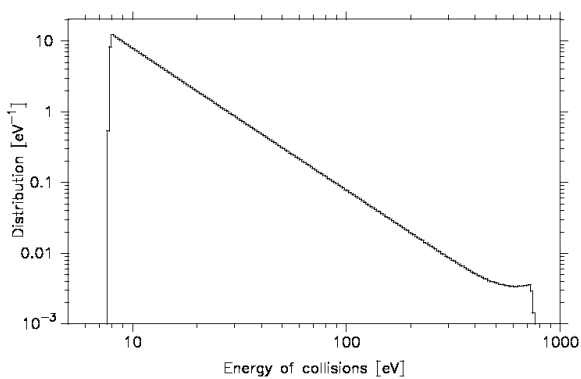


Fig.7:

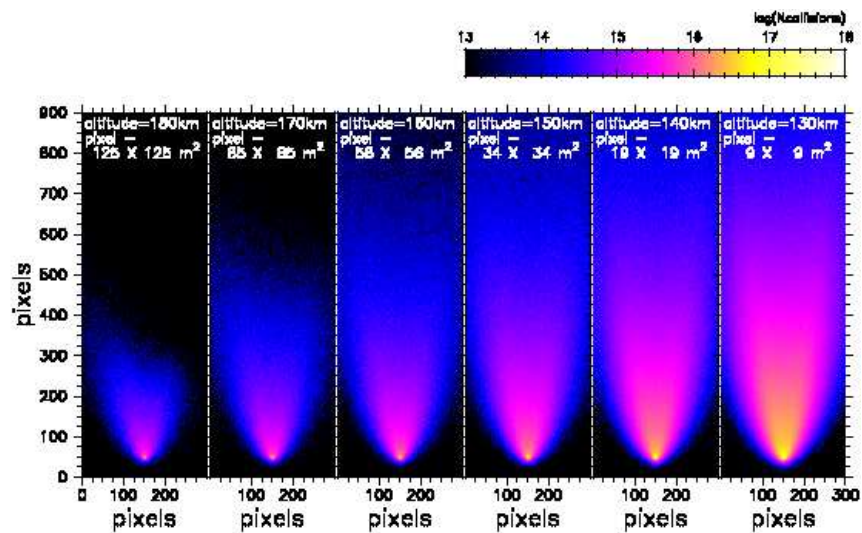


Fig.8:

